The Plant Cell, Vol. 21: 3672–3685, November 2009, www.plantcell.org © 2009 American Society of Plant Biologists

GNOM-LIKE1/ERMO1 and SEC24a/ERMO2 Are Required for Maintenance of Endoplasmic Reticulum Morphology in *Arabidopsis thaliana* [W]

Ryohei Thomas Nakano,[a] Ryo Matsushima,[a,1] Haruko Ueda,[a] Kentaro Tamura,[a] Tomoo Shimada,[a] Lixin Li,[a,2] Yasuko Hayashi,[b] Maki Kondo,[c] Mikio Nishimura,[c] and Ikuko Hara-Nishimura[a,3]

[a] Department of Botany, Graduate School of Science, Kyoto University, Kyoto 606-8502, Japan
[b] Department of Environmental Science, Faculty of Science, Niigata University, Niigata 950-2181, Japan
[c] Department of Cell Biology, National Institute for Basic Biology, Okazaki 444-8585, Japan

The endoplasmic reticulum (ER) is composed of tubules, sheets, and three-way junctions, resulting in a highly conserved polygonal network in all eukaryotes. The molecular mechanisms responsible for the organization of these structures are obscure. To identify novel factors responsible for ER morphology, we employed a forward genetic approach using a transgenic *Arabidopsis thaliana* plant (GFP-h) with fluorescently labeled ER. We isolated two mutants with defects in ER morphology and designated them *endoplasmic reticulum morphology1* (*ermo1*) and *ermo2*. The cells of both mutants developed a number of ER-derived spherical bodies, ~1 μm in diameter, in addition to the typical polygonal network of ER. The spherical bodies were distributed throughout the *ermo1* cells, while they formed a large aggregate in *ermo2* cells. We identified the responsible gene for *ermo1* to be *GNOM-LIKE1* (*GNL1*) and the gene for *ermo2* to be *SEC24a*. Homologs of both GNL1 and SEC24a are involved in membrane trafficking between the ER and Golgi in yeast and animal cells. Our findings, however, suggest that GNL1/ERMO1 and SEC24a/ERMO2 have a novel function in ER morphology in higher plants.

INTRODUCTION

The endoplasmic reticulum (ER) has the largest surface area among organelles in eukaryotic cells and forms diverse structures. The complex ER morphology supports diverse cellular functions, including synthesis of proteins and lipids, maintenance of calcium homeostasis, and quality control of proteins. There are three types of ER: rough ER, smooth ER, and nuclear envelope (Okita and Rogers, 1996; Staehelin, 1997; Baumann and Walz, 2001). The outer nuclear envelope is continuous with the rough ER, and the rough ER is distinguished from smooth ER by the presence of ribosomes on the cytosolic side of the membrane. The ER forms a dynamic polygonal network composed of tubules, sheets, and three-way junctions. In addition to these highly conserved structures, some organisms develop characteristic ER-derived structures. For example, *Brassicaceae* plants and some related species develop cylindrical structures called ER bodies that accumulate large amounts of β-glucosidase (PYK10), which may be involved in plant defense (Matsushima et al., 2002; Hara-Nishimura et al., 2004).

The cytoskeleton and molecular motors maintain ER morphology. Both microtubules and actin filaments are involved in the organization and dynamics of the ER in *Saccharomyces cerevisiae* (Prinz et al., 2000; Estrada et al., 2003), whereas microtubules are responsible for ER morphology in animal cells (Dabora and Sheetz, 1988; Waterman-Storer and Salmon, 1998). In *S. cerevisiae*, for example, recent studies have identified several factors that are involved in the maintenance and inheritance of the ER, including the kinesin motor Kar3p (Estrada de Martin et al., 2005b) and the myosin motor Myo4p (Estrada et al., 2003; Estrada de Martin et al., 2005b). A membrane protein, reticulon (RTN), and an AAA-ATPase, p97/CDC48, are also involved in maintaining the ER network. RTN is localized to the ER tubules and is responsible for the high curvature of the ER membrane in the tubules (Dreier and Rapoport, 2000; Voeltz et al., 2006; Hu et al., 2008; Shibata et al., 2008). p97 regulates homotypic membrane fusion in the ER, which is important for maintaining the ER network (Uchiyama et al., 2002, 2006; Kano et al., 2005). Actin filaments are crucial for organizing the ER network in plant cells (Estrada de Martin et al., 2005a; Tamura et al., 2005). However, the molecular mechanisms underlying the formation and maintenance of these ER structures remain poorly understood in plants.

In plant cells, unlike in yeast and animal cells, the ER network is widely distributed in a narrow space of cytoplasm between the plasma membrane and vacuolar membrane. This makes the plant cell a good model for observing the fine structure of the ER network by confocal microscopy (see Supplemental Figure 1 online). Additionally, the presence of a large central vacuole in each plant cell provides high optical transparency, which facilitates viewing of the intracellular structures of living cells.

[1] Current address: Research Institute for Bioresources, Okayama University, Kurashiki 710-0046, Japan.
[2] Current address: College of Life Science, Northeast Forestry University, Harbin 150040, China.
[3] Address correspondence to ihnishi@gr.bot.kyoto-u.ac.jp.
The author responsible for distribution of materials integral to the findings presented in this article in accordance with the policy described in the Instructions for Authors is: Ikuko Hara-Nishimura (ihnishi@gr.bot.kyoto-u.ac.jp).
[W] Online version contains Web-only data.
www.plantcell.org/cgi/doi/10.1105/tpc.109.068270

In this study, we employed a forward genetic approach using a model plant, *Arabidopsis thaliana*, to identify novel factors responsible for organizing and maintaining ER structures. Here, we report the isolation and characterization of two mutants (termed *endoplasmic reticulum morphology1* [*ermo1*] and *ermo2*) in which the ER morphology is abnormally organized.

RESULTS

ermo Mutants

An *Arabidopsis* transgenic plant, GFP-h, which expresses ER-localized green fluorescent protein (GFP), is a useful tool for visualizing the ER morphology within living cells (Figures 1A and 1B; see Supplemental Figure 1 online). We chemically mutagenized 4000 GFP-h seeds and obtained 1746 M2 lines. By observing 7-d-old seedlings of the M2 lines with a fluorescence microscope, we isolated two recessive mutants that had disorganized ER morphology (Figures 1C to 1F) and designated them *ermo1* and *ermo2*.

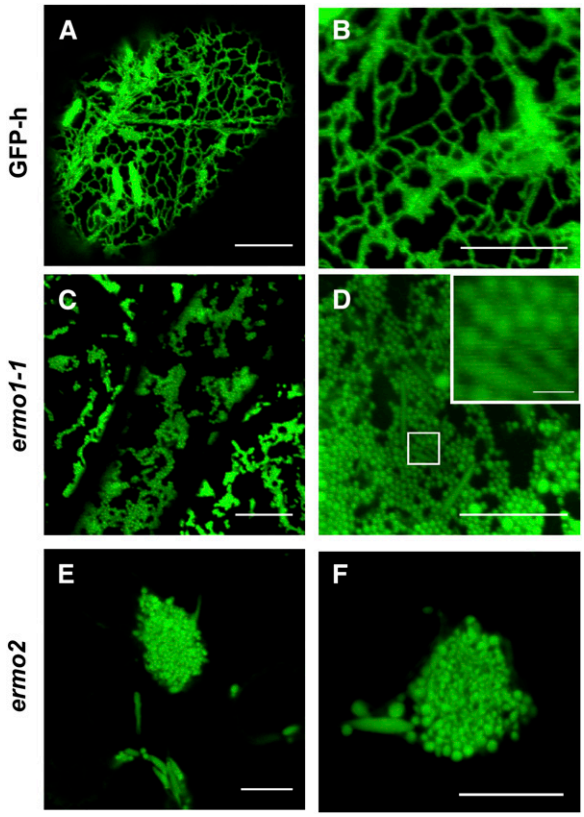

Figure 1. Abnormal Development of a Large Number of ~1-μm-Diameter Spherical Bodies in Both *ermo1-1* and *ermo2* Cells.

Two mutants that showed defects in ER morphology (*ermo1-1* and *ermo2*) were isolated from an ethyl methanesulfonate–mutagenized GFP-h pool. Both *ermo1-1* and *ermo2* developed a number of abnormal spherical bodies within the cells. Cotyledons (**[A]**, **[B]**, **[E]**, and **[F]**), petioles **(D)**, and hypocotyls **(C)** of *ermo1-1*, *ermo2*, and GFP-h plants were observed using a confocal laser scanning microscope. The inset in **(D)** shows the enlarged view of the boxed area. Bars = 10 μm in **(A)** to **(F)** and 1 μm in inset in **(D)**.

Both *ermo1* and *ermo2* developed a number of strongly GFP-labeled spherical structures that were ~1 μm in diameter (Figures 1C to 1F; see Supplemental Figures 2 and 3 online) and were not seen in the parental GFP-h. Increasing the detector gain of the microscope revealed that both mutants normally developed a polygonal network of ER (see Supplemental Figures 2H and 3F online) in addition to the spherical structures, which we designated as spherical bodies. *ermo1* had dispersed spherical bodies throughout the cells (Figures 1C and 1D), while *ermo2* had a single large aggregate of spherical bodies in each cell (Figures 1E and 1F) together with dispersed spherical bodies in the periphery of the cell (see Supplemental Figure 3E online). These phenotypes were seen in all tissues of *ermo1* and *ermo2* seedlings, including cotyledons, petioles, hypocotyls, and roots (see Supplemental Figures 2 and 3 online). In 10-d-old plants, a large fraction of the spherical bodies in cotyledon epidermal cells had disappeared (see Supplemental Figures 4A to 4P online). The spherical bodies were observed in young rosette leaves of these plants. However, in rosette leaves of 6-week-old plants, almost all spherical bodies had disappeared in both *ermo1* and *ermo2*, although *ermo2* still developed aggregates of spherical bodies within the cell (see Supplemental Figures 5A to 5C online). Taken together, these results indicate that the spherical bodies were present in young cells and gradually disappeared with age. We noticed that the spherical bodies did not form any aggregates in the young *ermo2* cells (see Supplemental Figure 6 online), indicating that the abnormal formation of the spherical bodies was not the trigger of aggregation. Despite the severe defects in ER morphology in young seedlings, the *ermo1* and *ermo2* mutants showed no gross morphological defects in 9-d-old seedlings (see Supplemental Figure 7A online) or in 8-week-old plants (see Supplemental Figure 7B online).

To determine the nature of the spherical bodies, organelles in 6- to 8-d-old seedlings of *ermo1* and *ermo2* were visualized either by transient expression of organelle-specific markers, KAM1ΔC-monomeric red fluorescent protein (mRFP) for Golgi (Tamura et al., 2005), Ara6-mRFP for endosomes (Ueda et al., 2004), and mRFP-PTS1 for peroxisomes (Tamura et al., 2005), or by chemical staining with 4',6-diamidino-2-phenylindole (DAPI) for nuclei and MitoTracker-Red for mitochondria. All of these organelles were distinct from the GFP-labeled spherical bodies in *ermo1* and *ermo2* (see Supplemental Figure 8 online). The *ermo2* aggregates were composed of not only spherical bodies but also other organelles, suggesting that *ermo2*, but not *ermo1*, has a defect in the intracellular distribution of these organelles (see Supplemental Figures 8M to 8O online).

Figure 2 shows electron micrographs of the epidermal cells of 7-d-old cotyledons from *ermo1* and *ermo2* plants. The *ermo1* cells developed many ~1-μm structures (Figures 2C to 2F), which were not seen in GFP-h cells (Figures 2A and 2B), suggesting that these abnormal structures correspond to the fluorescent spherical bodies of *ermo1* (Figures 1C and 1D). By contrast, each *ermo2* cell had a large aggregate that

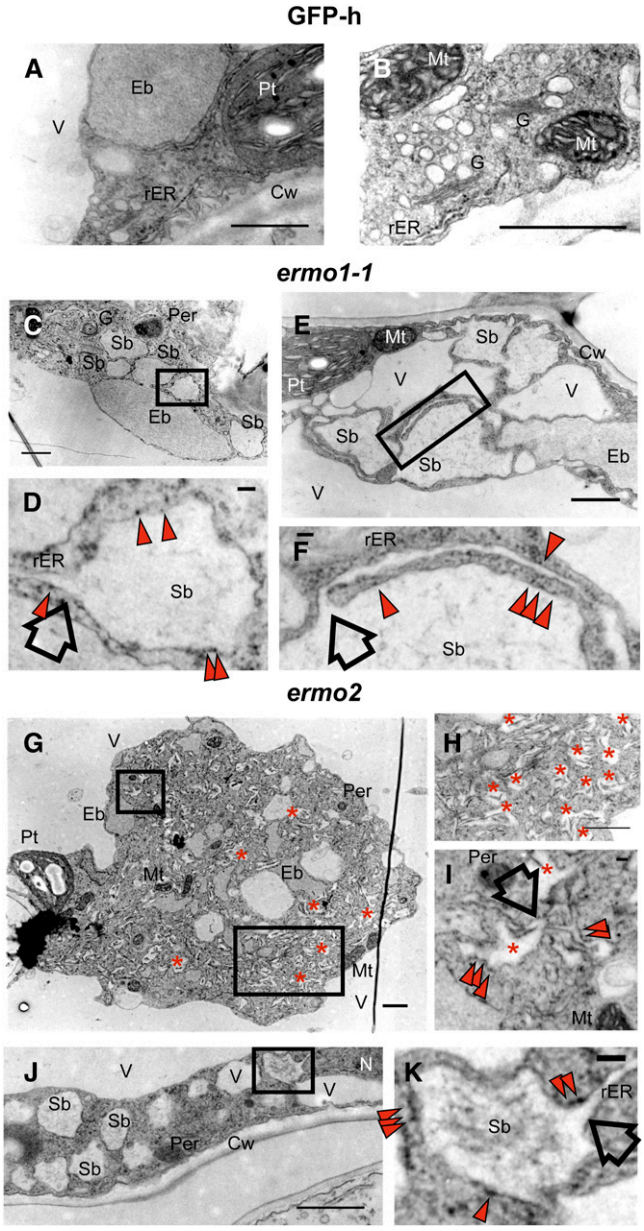

Figure 2. Spherical Bodies of *ermo1-1* and *ermo2* Are ER-Derived Structures.

Seven-day-old plants were subjected to ultrastructural analysis. Sb, spherical body; Eb, ER body; rER, rough ER; G, Golgi body; V, vacuole; N, nucleus; Mt, mitochondrion; Pt, plastid; Per, Peroxisome; Cw, cell wall.

(A) and **(B)** Cotyledon epidermal cells of a GFP-h plant.

(C) to **(F)** Cotyledon epidermal cells of a *ermo1-1* plant. **(D)** and **(F)** are enlarged views of **(C)** and **(E)**, respectively. Note that the spherical bodies were surrounded by ribosomes (arrowheads). Arrows indicate that spherical bodies were connected to the tubular rER.

(G) to **(K)** Cotyledon epidermal cells of *ermo2*. **(H)** and **(I)** are enlarged views of **(G)**, and **(K)** is an enlarged view of **(J)**. The spherical bodies were found both in the aggregate (**[G]** to **[I]**; indicated by red asterisks) and the periphery of the cells (**[J]** and **[K]**). The spherical bodies in *ermo2* were also surrounded by ribosomes (arrowheads) and connected to the tubular rER (arrows).

Bars = 1 μm in **(A)** to **(C)**, **(E)**, **(G)**, **(H)**, and **(J)** and 100 nm in **(D)**, **(F)**, **(I)**, and **(K)**.

contained many abnormal structures (red asterisks in Figures 2G to 2I), together with the other organelles, including mitochondria, peroxisomes, and ER bodies. In the periphery of *ermo2* cells, ~1 μm structures, which were similar to those in *ermo1* cells, were observed in the cytoplasm (Figures 2J and 2K). Neither the aggregates nor the ~1-μm structures were observed in GFP-h cells (Figures 2A and 2B), suggesting that the abnormal structures correspond to the fluorescent spherical bodies in *ermo2* cells (Figures 1E and 1F). The ~1-μm structures in both *ermo1* (Figures 2D and 2F) and *ermo2* (Figures 2I and 2K) were surrounded by ribosomes (indicated by arrowheads) and were occasionally connected to the tubular ER (indicated by arrows). These results suggest that the structures were derived from the ER and that they were not an abnormal accumulation of COPII vesicles or some other post-ER compartment.

Maintenance of Spherical Bodies in *ermo1* and *ermo2* Is Independent of Actin Microfilaments

Actin microfilaments (MFs) are involved in the maintenance of the ER network in higher plants (Tamura et al., 2005). To determine the contribution of MF to abnormal formation of the spherical bodies in *ermo1*, *ermo2*, and GFP-h plants, we visualized MF in these mutants with tdTomato-ABD2, the actin binding domain 2 of *Arabidopsis* Fimbrin 1 (ABD2 At Fim1; Higaki et al., 2007) fused to a RFP (tdTomato) (Figure 3). The ER network pattern was highly correlated with the MF pattern in GFP-h cells (Figures 3A and 3B). Similarly, both *ermo1* and *ermo2* had a normal MF network, and the distribution of the spherical bodies had a high correlation with the MF distribution (Figures 3C to 3E). Figures 3M and 3N show time-lapse image sequences of *ermo1* and *ermo2*, respectively. The spherical bodies moved along the actin filaments (see Supplemental Movies 1 and 2 online). These results suggest that the spherical bodies can interact with MF as does the typical ER network in wild-type plants.

Latrunculin B (Lat B), an actin polymerization inhibitor, disrupts the organization of endomembranes, including the ER, leading to the formation of endomembrane aggregates (Tamura et al., 2005). When GFP-h seedlings were treated with Lat B, similar aggregations appeared (Figures 3G and 3H, arrowheads). Lat B did not affect the maintenance of the spherical bodies in *ermo1* and *ermo2* and induced endomembrane aggregates in these mutants (Figures 3I to 3K, arrowheads). Lat B also did not affect the formation or maintenance of *ermo2* aggregates (Figure 3L, arrow), although the *ermo2* aggregates were surrounded by MFs (Figures 3F and 3F'). Additionally, the Lat B–induced aggregates were distinct from the *ermo2* aggregates of spherical bodies (Figure 3L, compare with 3K). These results suggest that MFs are not involved either in the maintenance of spherical bodies in

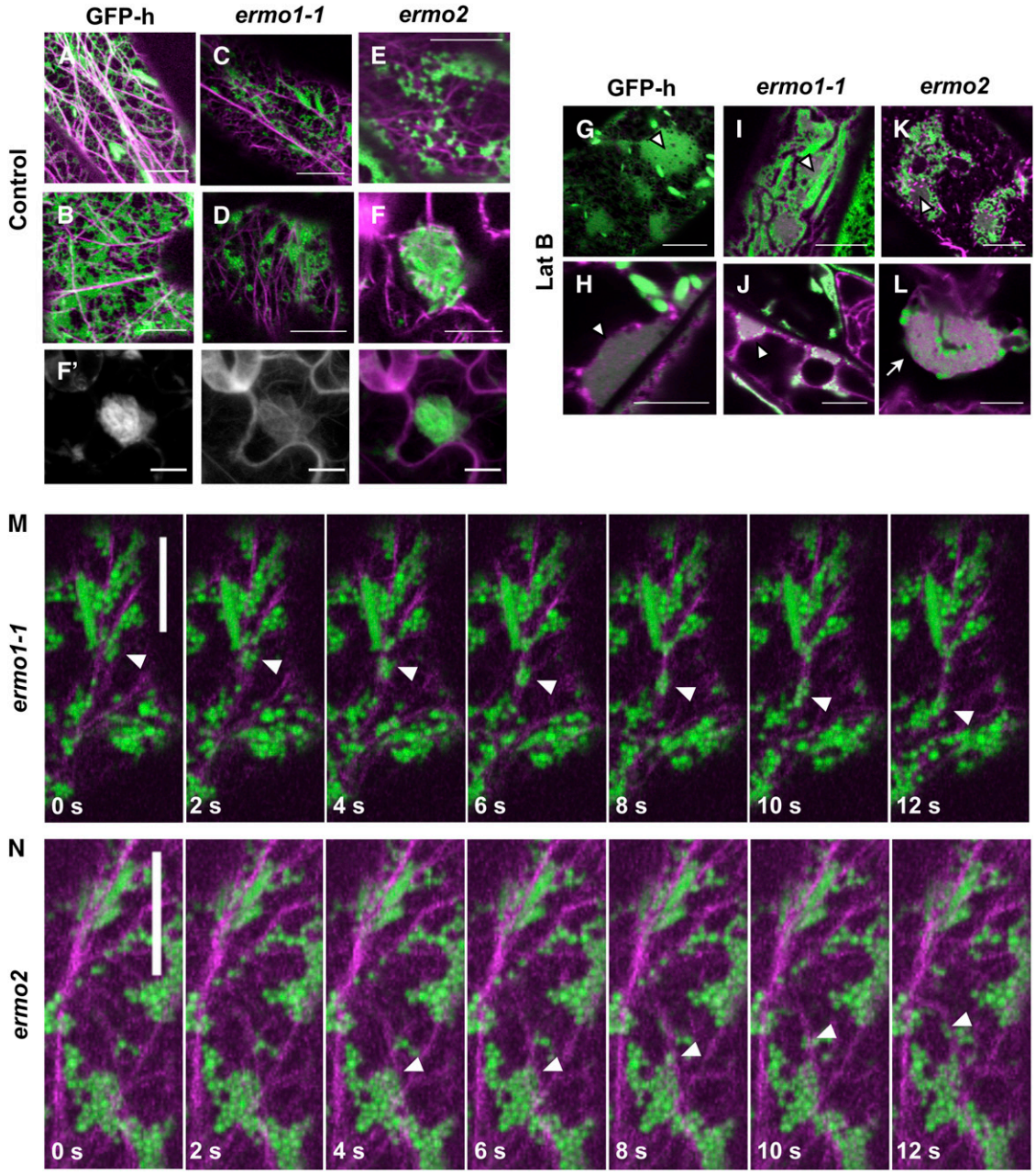

Figure 3. Maintenance of Spherical Bodies in *ermo1-1* and *ermo2* Is Independent of Actin Filaments.

GFP-h and *ermo* mutants were transformed with tdTomato-ABD2 to visualize actin filaments (magenta). Bars = 10 μm.

(A) to **(F')** In GFP-h cells (**[A]** and **[B]**), a large fraction of the ER (green) colocalized with actin filaments, shown as white signals. Typical networks of actin filaments were seen in *ermo1-1* (**[C]** and **[D]**) and *ermo2* (**[E]** and **[F]**) cells, and the spherical bodies were distributed along thick actin bundles (**[C]** to **[E]**). The aggregation of spherical bodies in *ermo2* was surrounded by actin filaments **(F)**. A three-dimensional reconstruction of **(F)** is shown in **(F')**. The single-channel SP-GFP-HDEL (left), tdTomato-ABD2 (center), and merged (right) images are shown.

(G) to **(L)** Seedlings of the transformants were treated with 100 μM Lat B for 2 h. In GFP-h cells (**[G]** and **[H]**), the ER network collapsed and formed aggregations (arrowheads). The spherical bodies in *ermo1-1* (**[I]** and **[J]**) and *ermo2* **(K)** cells were maintained in the presence of Lat B, and typical Lat B–induced aggregates were formed (arrowheads). The formation of spherical body aggregates in *ermo2* was not affected (**[L]**, arrow).

(M) and **(N)** Time-lapse image sequences of cotyledon epidermal cells of *ermo1-1* **(M)** and *ermo2* **(N)**. The spherical bodies in each mutant moved along the actin bundle (arrowheads).

ermo1 and *ermo2* mutants or in the aggregation of the spherical bodies in the *ermo2* cells.

Double Mutants of *ermo1* and *ermo2*

To determine whether there is a genetic interaction between *ERMO1* and *ERMO2*, we generated an *ermo1* and *ermo2* double mutant and observed the phenotype of the plant cells under a confocal microscope (Figure 4). The *ermo1 ermo2* cells developed a number of spherical bodies in the epidermal cells of cotyledons, hypocotyls, petioles, and roots of 7-d-old seedlings, similar to *ermo1* and *ermo2* cells. However, *ermo1 ermo2* cells did not form aggregates of spherical bodies in the cell. In 10-d-old seedlings, the spherical bodies were still visible in cotyledon epidermal cells and in those of rosette leaves (see Supplemental Figures 4Q to 4T online). Unlike single mutants, the *ermo1 ermo2* mutant retained the spherical bodies even in the rosette leaves of 6-week-old plants (see Supplemental Figure 5D online). The remaining spherical bodies did not form any aggregates. The spherical bodies of *ermo1 ermo2* plants were indistinguishable from those of *ermo1* or *ermo2* mutants, suggesting that spherical bodies of *ermo1* and *ermo2* might be equivalent to each other. These results indicate that *ermo1* and *ermo2* have synergistic effects on ER morphology and that *ermo1* has an epistatic effect on organelle distributions in the cell. ERMO1 and ERMO2 may have related roles in maintaining ER morphology and organelle distribution.

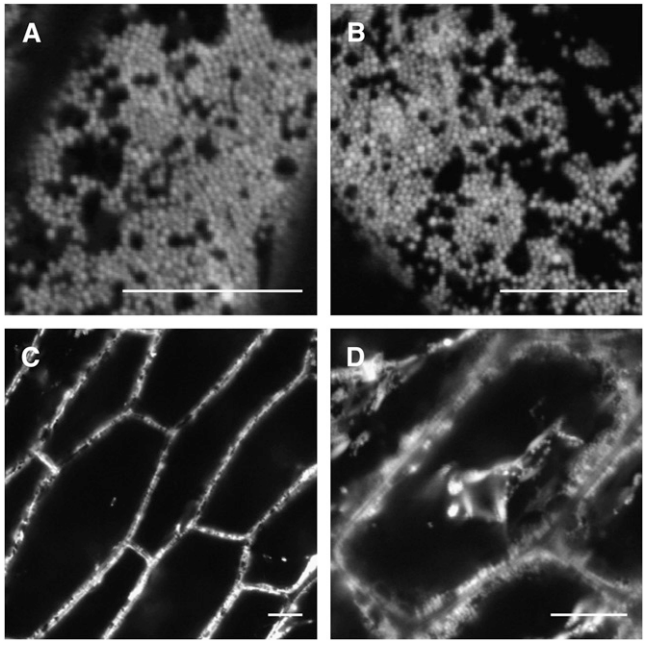

Figure 4. The Phenotype of the *ermo1-1 ermo2* Double Mutant.

Confocal images of the *ermo1-1 ermo2* double mutant. Seven-day-old seedlings were observed using a confocal microscope. Bars = 10 μm.
(A), **(C)**, and **(D)** Epidermal cells of the hypocotyl.
(B) Epidermal cells of the petiole. Note that the double mutant did not develop any aggregations of spherical bodies.

ERMO1 Encodes GNOM-LIKE1, a *cis*-Golgi-Localized ARF-GEF

Map-based cloning and DNA sequencing identified a single base pair mutation (C10T) that causes a nonsense mutation from CAG (Gln-4) to TAG (stop codon) in the *GNOM-LIKE1* (*GNL1*) locus of *ermo1* (Figure 5A). To confirm that the mutation is responsible for the *ermo1* phenotype, we established three homozygous T-DNA insertion lines (SALK_067415, SALK_091078, and SALK_030701) (Figure 5A). We named the originally isolated mutant *ermo1-1* and the T-DNA lines *ermo1-2*, *ermo1-3*, and *ermo1-4* (Figure 5A). To visualize the ER, an ER-targeted GFP construct was transiently expressed in 6- to 8-d-old seedlings of each T-DNA line. All of these lines developed spherical bodies similar to those in *ermo1-1* (Figures 5B to 5E). In addition, the F1 seedlings generated by crossing *ermo1-1* with either *ermo1-3* or *ermo1-4* also developed spherical bodies (Figures 5F and 5G, respectively). These results indicate that *ERMO1* is the gene that encodes GNL1.

GNL1 is a member of a large ARF-GEF (guanine nucleotide exchange factor for ADP-ribosylation factor) family (Richter et al., 2007; Teh and Moore, 2007). ARF-GEFs activate ARF, a small GTPase, which recruits various effector proteins. Similarly, GNL1 activates ARF proteins to initiate the formation of COPI vesicles, which are responsible for retrograde transport from the Golgi to ER (see Supplemental Figure 9 online). The *gnl1* mutant exhibits expanded diameters in Golgi bodies and exhibits hypersensitivity to the ARF-GEF inhibitor brefeldin A (BFA; Klausner et al., 1992). The mutant also exhibits defects in recycling of PIN-FORMED2 (PIN2) and secretion of secGFP (Richter et al., 2007; Teh and Moore, 2007). Teh and Moore (2007) observed abnormal structures that contain ER marker proteins in *gnl1* cells, which they called *gnl1* bodies, although the nature and the biogenesis of *gnl1* bodies were not investigated.

An RT-PCR analysis failed to detect normal GNL1/ERMO1 mRNA in *ermo1-2*, *ermo1-3*, or *ermo1-4*, indicating that that *ermo1-2*, *ermo1-3*, and *ermo1-4* are null mutants (Figure 5H). By contrast, mRNA was detected in *ermo1-1* and GFP-h plants (Figure 5H). This result suggests that *ermo1-1* cells may translate an abnormal ERMO1 protein lacking some N-terminal amino acids from an mRNA generated using a downstream ATG as an alternative start codon. The *ermo1-1* mutant may exhibit a milder phenotype in the plant and more normal seedling growth and less sensitivity to BFA (see Supplemental Figure 7 online; discussed below) than the other mutants as a result of producing an abnormal ERMO1 protein.

BFA Induces the Formation of Spherical Structures by Inhibiting GNL1/ERMO1 Function

GNOM, a homolog of GNL1/ERMO1, recycles membrane proteins from endosomes to the plasma membrane. A deficiency in GNOM causes abnormal localization of PIN1 proteins, the efflux carriers for auxin, resulting in severe defects during embryo development (Mayer et al., 1991, 1993). Recent studies have shown that GNL1/ERMO1 and GNOM exhibit functional redundancy in ER-Golgi transport as well

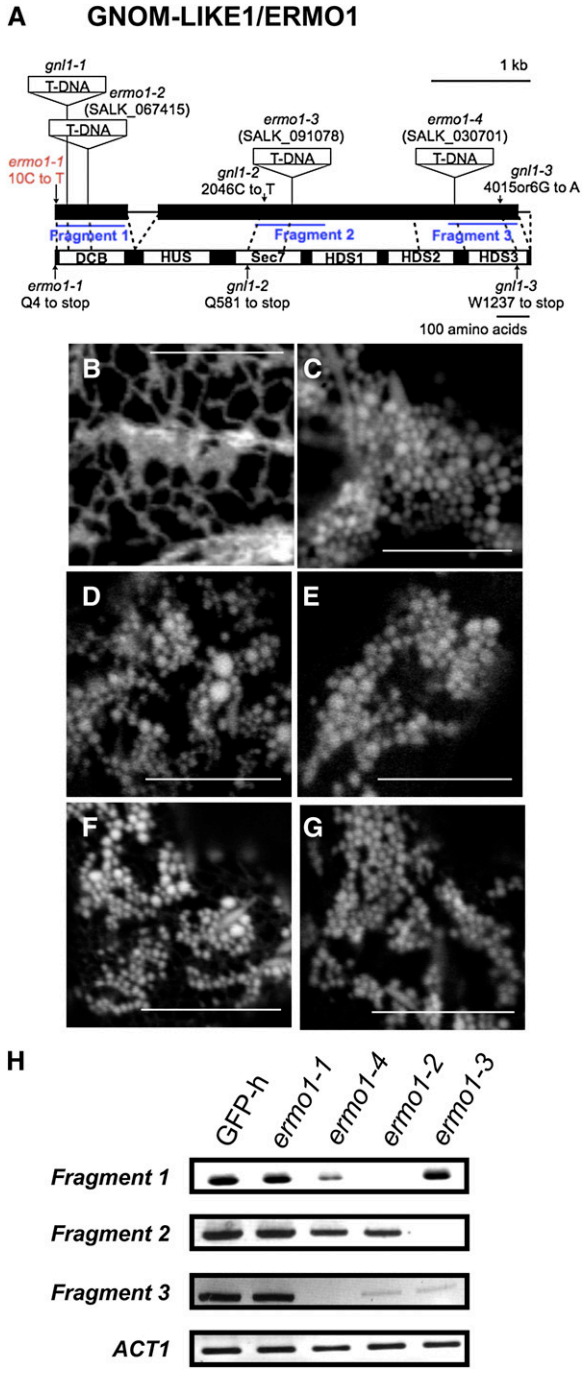

Figure 5. Identification of the *ERMO1/GNL1* Gene as Being Responsible for the *ermo1* Mutation.

(A) Positional cloning and DNA sequencing identified a mutation in the *GNL1* locus of *ermo1-1*. Mutation sites of T-DNA–inserted *ermo1* alleles and previously reported *gnl1* mutants are also shown. Black boxes and black lines indicate exons and introns, respectively. ERMO1/GNL1 has several characteristic domains: DCB, dimerization/cyclophilin binding domain; HUS, homology upstream of Sec7 domain; Sec7, Sec7 domain; HDS, homology downstream of Sec7 domain.

(B) to **(E)** SP-GFP-HDEL was transiently expressed in T-DNA insertion lines. Confocal images of the ER in GFP-h **(B)**, *ermo1-2* **(C)**, *ermo1-3* **(D)**, and *ermo1-4* **(E)** cells are shown. Bars = 10 μm.

(F) and **(G)** Confocal images of F1 plants generated by crossing *ermo1-1* with either *ermo1-3* **(F)** or *ermo1-4* **(G)**. All the T-DNA insertion lines and the F1 lines showed abnormal ER morphology identical to the phenotype of *ermo1-1*. Bars = 10 μm.

(H) RT-PCR analysis revealed that *GNL1* mRNA was not transcribed in T-DNA insertion mutant alleles, with the exception of *ermo1-1*. Amplified regions are indicated by blue lines in **(A)**. Two biological replicates were performed.

as in the endocytotic pathways (Richter et al., 2007; Teh and Moore, 2007). To determine whether GNOM functions in maintaining ER morphology as does GNL1/ERMO1, we used BFA to inhibit GNOM function. BFA, at a concentration of 25 μg/mL, does not inhibit GNL1, but does inhibit the BFA-sensitive ARF-GEFs, including GNOM (Richter et al., 2007; Teh and Moore, 2007). BFA treatment resulted in the formation of BFA compartments that are composed of endosomal components (Satiat-Jeunemaitre et al., 1996; Wee et al., 1998; Baldwin et al., 2001; Tse et al., 2004). When seedlings of a transgenic plant that expresses the *trans*-Golgi marker ST-GFP (Saint-Jore et al., 2002) were treated with BFA (25 μg/mL), BFA compartments were formed (Figures 6C and 6D). This result indicates that GNOM function was inhibited by 25 μg/mL of BFA. However, 25 μg/mL of BFA did not cause any defects in ER morphology in the GFP-h seedlings (Figures 6A and 6B). These results indicate that GNOM is not required for maintaining ER morphology and that GNL1/ERMO1 alone is sufficient to maintain ER morphology.

Interestingly, a higher concentration of BFA (100 μg/mL) induced the formation of spherical structures similar to the spherical bodies present in *ermo1* plants (Figures 6E to 6H), suggesting that this concentration of BFA inhibited GNL1/ERMO1. Furthermore, the ST-GFP was redistributed to the ER as a result of the inhibition of ER-Golgi transport by BFA, as observed in *gnl1* mutants treated with 25 μg/mL of BFA (Figure 6I; Richter et al., 2007; Teh and Moore, 2007). To further confirm that the formation of spherical structures resulted from the inhibition of GNL1/ERMO1 tobacco (*Nicotiana tabacum*) Bright Yellow 2 suspension-cultured cells expressing SP-GFP-HDEL were treated with 10 μg/mL of BFA, which induces the redistribution of Golgi-localized proteins to the ER in Bright Yellow 2 cells (Ritzenthaler et al., 2002). The 10-μg/mL BFA treatment resulted in the formation of spherical structures that were similar to those seen in GFP-h plants treated with 100 μg/mL BFA (cf. Supplemental Figure 10 online with Figures 6E and 6F), suggesting that formation of spherical structures by BFA was not due to a secondary effect resulting from the high concentration of BFA but to the inhibition of GNL1/ERMO1. The BFA-induced spherical structures often formed several aggregates within a single cell (Figure 6G). These aggregates were always associated with the BFA compartments that were labeled with the fluorescent dye FM4-64 (Figure 6H), suggesting that the aggregates may be formed by inhibiting BFA-sensitive ARF-GEFs rather than by inhibiting GNL1/ERMO1.

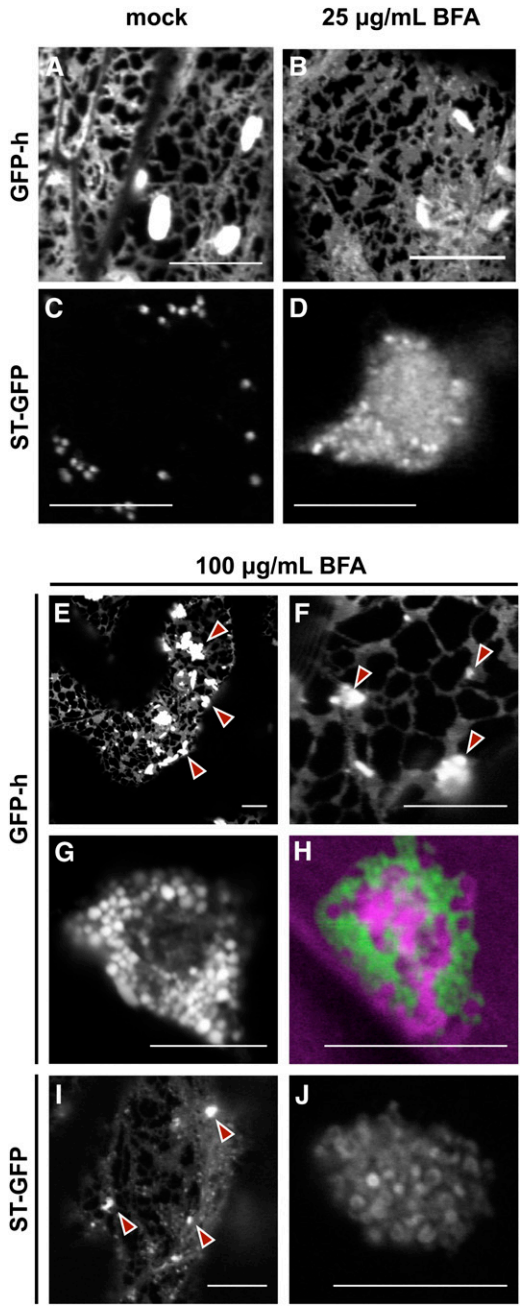

Figure 6. A High Concentration of BFA Induces Abnormal Structures Similar to the Spherical Bodies of *ermo1-1* and *ermo2* Plants.

(A) to **(D)** Seedlings of GFP-h (**[A]** and **[B]**) and ST-GFP (**[C]** and **[D]**) plants were treated with either 25 μg/mL BFA (**[B]** and **[D]**) or solvent control (**[A]** and **[C]**). BFA (25 μg/mL) induced BFA compartments, which were visualized with ST-GFP **(D),** but did not affect ER morphology **(B)**.
(E) to **(J)** Seedlings of GFP-h (**[E]** to **[H]**) or ST-GFP (**[I]** and **[J]**) plants were treated with 100 μg/mL BFA. Bars = 10 μm.
(E) and **(F)** The treatment induced GFP fluorescent spherical structures that were similar to the spherical bodies in *ermo1* mutants (arrowheads).
(G) The spherical structures occasionally formed several aggregations within a cell.
(H) The aggregations were associated with the BFA compartments that were visualized by FM4-64 (magenta).
(I) and **(J)** The BFA treatment caused a redistribution of ST-GFP to both the ER and the BFA compartments. Note that ST-GFP also showed GFP fluorescent spherical structures (arrowheads in **[I]**).

ERMO2 Encodes SEC24a, a Component of Coat Proteins of COPII Vesicles

Map-based cloning and DNA sequencing identified a single base pair mutation (G2078A) that causes a missense mutation from AGA (Arg-693) to AAA (Lys-693) in the *SEC24a* locus of *ermo2* (Figure 7A). To confirm that the mutation in *SEC24a* was responsible for the *ermo2* phenotype, we introduced a fusion gene composed of the *SEC24a* cDNA and the tdTomato cDNA into *ermo2* plants. The transgenic plants showed normal ER morphology (Figures 7B and 7C), indicating that the transgene rescued the *ermo2* defect. These results indicate that *ERMO2* is the gene that encodes SEC24a, which is a member of the coat protein complex of COPII vesicles responsible for anterograde transport from the ER to Golgi (see Supplemental Figure 9 online). The Arg residue, which is substituted with Lys in *ermo2*, is necessary for cargo binding in *S. cerevisiae* (Miller et al., 2003) and is conserved among Sec24 proteins from a variety of eukaryotes (Figure 7D). To determine whether the abnormal organization of the ER and abnormal organelle distributions are specific to the point mutation of SEC24a/ERMO2, we tried to isolate a homozygous T-DNA insertion line. However, we were unable to establish a homozygous line by self-crossing the heterozygous lines (GK_172F03). This result suggests that the defect in SEC24a/ERMO2 causes a severe defect in plant growth (Faso et al., 2009).

A Novel Function of GNL1/ERMO1 and SEC24a/ERMO2 in Maintaining ER Morphology

Both GNL1/ERMO1 and SEC24a/ERMO2 are thought to be involved in ER-Golgi transport (see Supplemental Figure 9 online). One possibility is that an imbalance in the import and export of proteins in the ER results in the formation of the spherical bodies. To examine this possibility, we inhibited protein synthesis in *ermo1-1* and *ermo2* plants using the ribosome inhibitor cycloheximide (CHX). CHX had no effect on ER morphology in GFP-h control plants (Figure 8A), and the reduction of protein import into the ER did not rescue the abnormal formation of spherical bodies in the mutants (Figures 8B to 8D). These data suggest that the accumulation of proteins in the ER is not responsible for the formation of spherical bodies in the *ermo1* and *ermo2* mutants.

To clarify the relationship between ER-Golgi transport and ER morphology, we focused on another mutant that has a defect in ER-Golgi transport. Previously, we reported that MAIGO2 (MAG2), which is a tethering factor for fusion events between COPI vesicles and the ER, is necessary for ER-Golgi transport. In *mag2* mutants, ER-Golgi transport was defective, and abnormal structures called MAG2 bodies developed in the mutant seed cells, while *mal* mutants, in which the closest homolog of *MAG2*

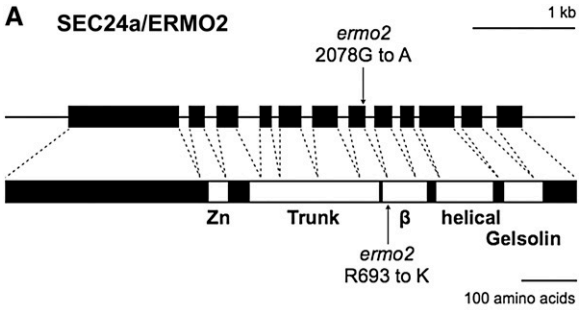

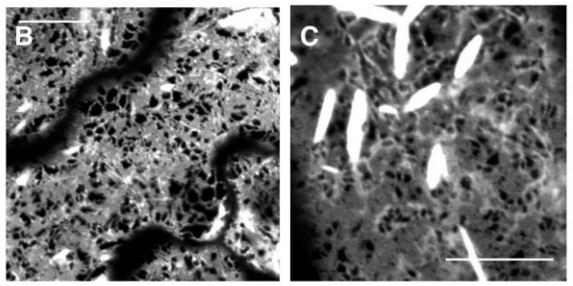

D

Pp Sec24A	VMRVRCSNG	672
Pp Sec24B	VMRVRCSNG	707
At SEC24b	VMRVRCSQG	762
At SEC24c	VMRVRCSQG	759
Os12g0430000	VMRVRCSQG	485
Hs SEC24D	IMRVRTSTG	698
Hs SEC24C	VMRVRTSTG	760
Hs SEC24B	VMRIRCTKG	756
Hs SEC24A	VMRIRCTKG	896
Dm Sec24	VMRIRCTRG	836
Pp Sec24C	VMRIRCGKG	514
Pp Sec24D	VMRIRCGKG	700
Os04g0129500	VMRIRCGKG	692
ERMO2/SEC24a	VMRIRCGKG	697
Sc Sec24p	VMRARGSTG	565
Sc Iss1p	VMRVRCSTG	521
Os05g0443300	VLRLRTSSD	408
At SEC24d	VLRLRTSTE	391
Sc Lst1p	LLKVRCSTG	549

Figure 7. Identification of the *SEC24a*/*ERMO2* Gene as Being Responsible for the *ermo2* Mutation.

(A) Positional cloning and DNA sequencing identified a mutation in the *SEC24a* locus of *ermo2*. Black boxes and black lines indicate exons and introns, respectively. SEC24a/ERMO2 has several characteristic domains: Zn, zinc finger domain; Trunk, Sec23/24 trunk domain; β, Sec23/24 β-sandwich domain; helical, Sec23/24 helical domain; Gelsolin, Gelsolin repeat domain.

(B) and **(C)** Independent *ermo2* lines transformed with tdTomato-SEC24a were observed using a confocal microscope. No visible defects in ER morphology were observed in the transformant lines, indicating that *SEC24a* was responsible for the *ermo2* phenotype. Bars = 10 μm.

(D) The amino acid (Arg) at the *ermo2* mutation site is completely conserved in SEC24 proteins from *Arabidopsis* (At), *Oryza sativa* (Os), *Physcomitrella patens* (Pp), *Homo sapiens* (Hs), *Drosophila melanogaster* (Dm), and *S. cerevisiae* (Sc). The last amino acid positions are indicated after each sequence. The residues corresponding to Arg-693 in *SEC24a*/*ERMO2* are indicated in red.

(*MAG2-LIKE* [*MAL*]) was defective, did not show any obvious defects in membrane trafficking (Li et al., 2006). To abolish MAG2 and MAL function, we generated a double mutant, *mag2-1 mal*, that was defective for both genes. The *mag2-1 mal* plants showed no defects in ER morphology (Figure 8E). This result suggests that ER-Golgi transport is not essential for maintaining ER morphology.

We next examined vacuolar protein transport in *ermo1-1* and *ermo2* plants, by monitoring the transport of the seed protein 12S globulin into protein storage vacuoles and RD21 into lytic vacuoles. Unexpectedly, however, we found no defects in the transport of either protein to the two different vacuoles (Figure 8F for protein storage vacuoles and 8G for lytic vacuoles). These results suggest that GNL1/ERMO1 and SEC24a/ERMO2 have a specific function in the proper organization and maintenance of ER morphology rather than in bulk transport of proteins between ER and Golgi or ER and vacuole.

DISCUSSION

The Spherical Body Is a Novel Structure Derived from the ER

Both GNL1/ERMO1 and SEC24a/ERMO2 are involved in membrane trafficking between the ER and Golgi (Hicke et al., 1992; Richter et al., 2007; Teh and Moore, 2007). Our findings show that GNL1/ERMO1 and SEC24a/ERMO2 function in suppressing the abnormal formation of spherical bodies from the ER, although their functions are distinct in how they affect the positioning of organelles within the cells. Our results suggest that the formation of abnormal structures from the ER results from a defect in membrane trafficking. Two kinds of ER-derived abnormal structures, 50-nm vesicles in *S. cerevisiae* (Kaiser and Schekman, 1990) and MAG2 bodies in *Arabidopsis* seeds (Li et al., 2006), have been shown to be induced by defects in ER-Golgi transport.

The 50-nm vesicles are formed in various *sec* mutants of *S. cerevisiae*, in which protein export from the ER is abolished (Kaiser and Schekman, 1990). Production of the vesicles is suppressed by inhibiting protein synthesis in the cells, indicating that the vesicles are induced by an imbalance in import and export of proteins in the ER. However, CHX did not affect the formation of spherical bodies in the *ermo* mutants (Figures 8A to 8D), suggesting that the import-export imbalance is not the primary trigger for the formation of spherical bodies.

MAG2 bodies, which develop from the ER in seeds of *mag2* mutants, are aggregates composed of the precursors of seed storage proteins, 2S albumins, that were actively synthesized in the ER during seed maturation. The diameter of MAG2 bodies (~1 μm) is comparable to that of the spherical bodies in the *ermo* mutants. Our finding, however, that the *mag2 mal* double mutant did not show any defect in ER morphology in seedlings (Figure 8E) suggests that the mechanism responsible for the formation of spherical bodies in *ermo* mutants differs from that of MAG2 bodies in seed cells.

Taken together, these results show that the spherical bodies are novel structures that are derived from the ER by a mechanism involving GNL1/ERMO1 and SEC24a/ERMO2. Faso et al. (2009) showed that the aggregate in the *sec24a* mutant was labeled with the fluorescent dye, DiOC6, showing that the phenotype was independent to the expression of ST-GFP. This result suggests that the abnormal formation of the spherical bodies

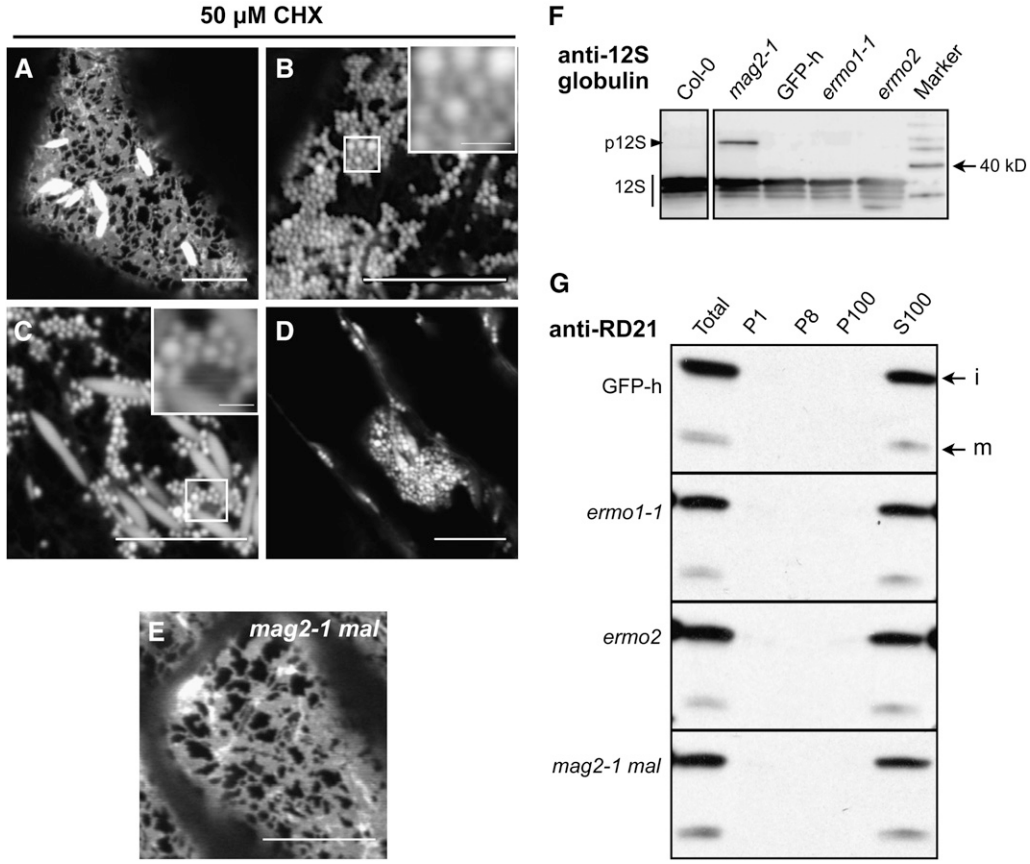

Figure 8. Abnormal Formation of the Spherical Bodies Is Not Caused by Defects in Protein Export from the ER.

(A) to **(D)** GFP-h **(A)**, *ermo1-1* **(B)**, and *ermo2* (**[C]** and **[D]**) cells were treated with 50 μM CHX for 2 h. Spherical bodies and aggregations were formed and maintained in the presence of CHX. The insets in **(B)** and **(C)** are enlarged views of the boxed area in each panel. Bars = 10 μm in **(A)** to **(D)** and 1 μm in insets in **(B)** and **(C)**.

(E) SP-GFP-HDEL was stably introduced into a *mag2-1 mal* double mutant. No defects in ER morphology were detected.

(F) Total protein from dry seeds was extracted and subjected to immunoblot analysis using anti-12S globulin antibodies. The *ermo1-1* and *ermo2* mutants did not accumulate precursors of 12S globulin (p12S), while *mag2-1* with a defect in ER-Golgi transport showed abnormal accumulation of precursor forms (arrowhead).

(G) Suborganeller fractionation using 3-week-old GFP-h, *ermo1-1*, *ermo2*, and *mag2-1 mal* plants followed by immunoblotting using anti-RD21 antibodies was performed. P1, P8, P100, and S100 fractions are rich in nuclei, plastids, microsomes, and soluble proteins, respectively. Both intermediate (i) and mature (m) forms of RD21 were detected in the vacuole-rich fraction (S100) in each mutant.

and the aggregations in *ermo2* do not depend on the overexpression of GFP fusion proteins.

The N Terminus Is Necessary for GNL1/ERMO1 to Maintain ER Morphology

The *ermo1-1* plants showed no defects in plant growth, while *ermo1-2*, *ermo1-3*, and *ermo1-4* exhibited a semidwarf phenotype (see Supplemental Figure 7 online). Since the three T-DNA insertion lines did not express normal *GNL1/ERMO1* mRNA (Figure 5H) and showed similar phenotypes (Figures 5C to 5E), they were thought to be null mutants. The *ermo1-1* plants may express an abnormal GNL1/ERMO1 protein with several amino acids in the N terminus deleted, and a partially functional abnormal protein could enable plant growth to appear normal. However, spherical bodies were formed in *ermo1-1* cells, which express the N terminus–deleted ERMO1, indicating that the N terminus of GNL1/ERMO1 is necessary to maintain ER morphology. The inhibition of GNL1/ERMO1 by BFA induced the formation of spherical structures from the ER (Figure 6; see Supplemental Figure 10 online). Since BFA blocks the interaction between ARF-GEF and ARF (Robineau et al., 2000; Renault et al., 2003; Zeghouf et al., 2005), the N terminus of GNL1/ERMO1 may be necessary for this interaction. Furthermore, these results suggest that the interaction between GNL1/ERMO1 and the target ARF proteins is necessary for normal ER morphology. Our finding that the milder phenotype in plant growth was seen even in the presence of BFA (see Supplemental Figure 7C online) indicates that the residual function of the abnormal GNL1/ERMO1 was not inhibited by BFA.

GNL1/ERMO1 and SEC24a/ERMO2 May Have Roles in Maintaining ER Morphology

Although we could not find any evidence for defects in the bulk transport of vacuolar proteins in the *ermo* mutants (Figures 8F and 8G), our results do not rule out the possibility that GNL1/ERMO1 and SEC24a/ERMO2 contribute to ER-Golgi transport. Plants can transport proteins from the ER into vacuoles both through Golgi-dependent and Golgi-independent pathways (Shimada et al., 2003; Li et al., 2006; Shimada et al., 2006; Fuji et al., 2007). Indeed, Teh and Moore (2007) reported that *gnl1* mutants, which are allelic to *ermo1* mutants, accumulate secretory GFP in the ER. In this study, we focused on vacuolar proteins because of the ease of monitoring the trafficking and/or processing of these proteins; however, we did not detect any defects in vacuolar trafficking. These differences between our study and the study of Teh and Moore (2007) may suggest that multiple pathways exist for trafficking from the ER to the vacuoles and for secretion. Therefore, it is possible that the novel mechanism underlying the formation of the spherical bodies reflects a membrane trafficking pathway.

Alternatively, GNL1/ERMO1 and SEC24a/ERMO2 may be involved in transport of some specific proteins, which are required for organizing ER morphology. In the sequence of vesicle budding events from the ER, SEC24a/ERMO2 directly binds cargo proteins to recruit them into COPII vesicles. Sec24p in *S. cerevisiae* has several cargo binding sites, each for a specific cargo (Miller et al., 2003). As described above, the direct trigger of the *ermo2* phenotype was suggested to be a point mutation in one of the cargo binding sites, the B-site. This observation suggests that the packaging of some specific cargo into COPII vesicles is impaired in *ermo2* and that the mis-sorted cargo is a key factor for maintaining ER morphology. However, GNL1/ERMO1 functions in the first step of COPI vesicle budding, suggesting a less specific interaction with cargo proteins. Since the defective retrograde transport may also cause partial defects in anterograde transport, the study of Teh and Moore (2007) showing that GNL1/ERMO1 contributes to retrograde transport suggests that protein export from the ER was also partially defective in *ermo1* mutants. Such defects could lead to partial mis-sorting of key factors, as in the *ermo2* mutant, and could induce the defects in ER morphology. This hypothesis is consistent with the relatively severe defects in the *ermo1-1 ermo2* double mutant. Since *Arabidopsis* has three isoforms of SEC24 proteins, according to the genome sequence information (Figure 7D), the other isoforms may partially rescue packaging of the key factors into COPII vesicles. When GNL1/ERMO1 and SEC24a/ERMO2 are both defective, the SEC24a-dependent pathway is blocked, and the SEC24b- and SEC24c-dependent pathways are partially disrupted because of the defects in retrograde transport. The isolation and characterization of specific cargos will be the subject of future studies.

In animal cells, ER tubules are stabilized by microtubules and interactions between a kinesin-type motor and CLIMP63 (cytoskeleton-linking ER membrane protein of 63 kD) result in homotypic fusion of the adjoining membranes of two ER tubules by the actions of p97, p22, and other cofactors (Vedrenne and Hauri, 2006). This result suggests that the cytoskeleton is involved in ER morphology. In *S. cerevisiae*, ER morphology is maintained by Kar3p and Ice2p (Estrada et al., 2003), and ER morphology during cell division is maintained by Myo4p and She3p (Estrada de Martin et al., 2005b). Rtn1p is involved in anchoring ER tubules beneath the plasma membrane by interacting with the exocyst complex (De Craene et al., 2006), which is responsible for exocytosis, and the membrane protein RTN, which maintains the high curvature of ER tubules (Voeltz et al., 2006). Similar mechanism may mediate the organization and maintenance of ER morphology in plant cells. For example, RTN is localized to the ER in plant cells, and its overexpression induces the remodeling of the ER network (Nziengui et al., 2007; Tolley et al., 2008). However, the ER-derived spherical body-like structures shown here have not been reported for any organism. Consequently, GNL1/ERMO1 and SEC24a/ERMO2 may regulate ER morphology in a manner that is unique to higher plants.

Spherical Bodies and Organelle Distribution in *ermo* Mutants

From our analysis using various organelle markers, we found that the distribution of organelles in the *ermo2* mutant differed from that of wild-type plants (see Supplemental Figure 8 online). The spherical bodies in *ermo2* plants may actively accumulate, and their aggregation may randomly entrap other organelles. Alternatively, a molecular mechanism to keep organelles properly distributed may be defective in *ermo2* mutants, resulting in random entrapment of organelles, including of the spherical bodies.

Previously, we reported that the *Arabidopsis* mutants *katamari1* (*kam1*) (Tamura et al., 2005) and *kam2* (Tamura et al., 2007) develop aggregations of organelles in the cell, similar to those in *ermo2*. KAM1, which is a Golgi-localized membrane protein, regulates the organization of the actin network by interacting with actin MF (Tamura et al., 2005), while KAM2 is involved in vacuolar protein transport in seeds (Tamura et al., 2007). These studies suggest that multiple molecular mechanisms may underlie organelle distributions. However, SEC24a/ERMO2 proteins are not involved in organizing the actin network (Figures 3E and 3F) or in vacuolar protein transport in seeds (Figure 8F). Additionally, neither *kam1* nor *kam2* develop spherical body-like structures. The *kam2* aggregates, in which FM4-64 positive endomembranes form sheet-like structures, are quite different from those in *ermo2*. Thus, our findings suggest that SEC24a/ERMO2 is involved in the subcellular distribution of organelles in a manner distinct from KAM1 and KAM2. Since young *ermo2* cells did not develop any aggregations, the presence of the spherical bodies does not appear to be a direct trigger for the formation of aggregations (see Supplemental Figure 6 online). We found that aged cells in which many spherical bodies had disappeared still developed the aggregates, suggesting that the components of the aggregates and the spherical bodies do not completely overlap.

Since the *ermo1-1 ermo2* double mutant did not develop aggregates of spherical bodies, *ermo1-1* is epistatic to *ermo2* in regard to organelle distribution. The result also indicates that GNL1/ERMO1 is involved in maintaining the organelle distribution in a manner related to SEC24a/ERMO2 function.

METHODS

Plant Materials and Growth Conditions

We used wild-type plants of *Arabidopsis thaliana* (ecotype Columbia [Col] and Landsberg *erecta*) and a transgenic plant of *Arabidopsis* (ecotype Col) called *GFP-h* that expresses SP-GFP-HDEL, which is composed of the signal peptide of pumpkin (*Cucurbita maxima*) 2S albumin, and GFP followed by an ER retention signal, HDEL (Mitsuhashi et al., 2000; Hayashi et al., 2001). *mag2-1* was obtained as reported previously (Li et al., 2006). Information about T-DNA insertion mutants, SALK_067415 (*ermo1-2*), SALK_091078 (*ermo1-3*), SALK_030701 *(ermo1-4*), and GK-288E12 (*mal*) was obtained from the Salk Institute Genomic Analysis Laboratory website (http://signal.salk.edu/). All seeds except for GK-288E12 were provided by the ABRC at Ohio State University. GK-288E12 was provided by the Nottingham Arabidopsis Stock Centre. Surface-sterilized seeds were sown onto 0.5% Gellan Gum (Wako) with Murashige and Skoog medium (Wako) supplemented with *myo*-inositol and 1% sucrose and were grown at 22°C under continuous light.

Isolation of *ermo* Mutants

GFP-h seeds were mutagenized as described previously (Matsushima et al., 2004). Six- to seven-day-old seedlings of each M2 line were examined with a fluorescence microscope (Axioskop 2 plus system; Carl Zeiss), and M2 lines that showed defects in ER morphology were selected. We named them *ermo* mutants. *ermo* mutants were crossed with *Arabidopsis* ecotype Landsberg *erecta*, and the genotype of *ermo* was analyzed using a combination of cleaved amplified polymorphic sequence and simple sequence length polymorphism markers (Konieczny and Ausubel, 1993; Bell and Ecker, 1994) with data obtained from The Arabidopsis Information Resource (http://www.arabidopsis.org) and NARAMAP markers, which were donated by M. Tasaka and M. Morita of the Nara Institute of Science and Technology.

Plasmid Constructions

The *Arabidopsis ABD2 Fim1* gene in the pUC18 vector was provided by S. Hasezawa of the University of Tokyo (Higaki et al., 2007). We amplified *ABD2* with specific primers cacc-ABD2-F and ABD2-stopR (see Supplemental Table 1 online) and subcloned the amplified fragment into pENTR/D-TOPO using Gateway TOPO cloning kit (Invitrogen). This DNA construct was introduced into the pB5tdGW plant expression vector by the LR reaction of the Gateway system (Invitrogen). pB5tdGW was donated by T. Nakagawa of Shimane University (Nakagawa et al., 2007).

The cDNAs for ERMO2/SEC24 were amplified by PCR from a cDNA library prepared from *Arabidopsis* roots using the primer pair Sec24F and Sec24R (see Supplemental Table 1 online). The amplified fragments were inserted into the *Bam*HI-*Xho*I site of pENTR3C (Invitrogen). This DNA construct was introduced into the pB5GWtd plant expression vector by LR reaction of the Gateway system (Invitrogen). pB5GWtd was donated by T. Nakagawa of Shimane University (Nakagawa et al., 2007).

A plant expression vector containing *ST-GFP* cDNA was donated by C. Hawes of Oxford Brookes University.

Each plant expression vector was introduced into *Agrobacterium tumefaciens* strain GV3101 by electroporation, and the transformed bacteria were then infiltrated into *Arabidopsis* ecotype Col plants by the floral dip method (Clough and Bent, 1998). The *tdTomato* gene and the Gateway vector of tdTomato were provided by R.Y. Tsien of Howard Hughes Medical Institute and S. Mano of National Institute for Basic Biology, respectively.

Isolation of RNA and RT-PCR

Total RNA was isolated from 8-d-old seedlings of GFP-h, *ermo1-1*, *ermo1-2*, *ermo1-3*, and *ermo1-4* with the RNeasy plant mini kit (Qiagen). cDNA was synthesized from total RNA with Ready-To-Go RT-PCR beads (GE Healthcare Bio-Science). PCR was performed with the cDNAs and ExTaq polymerase (TaKaRa), and products were visualized with ethidium bromide staining. Primer sets used are shown in Supplemental Table 1 online.

Transient Expression of RFP-Tagged Organelle Markers

Seven-day-old seedlings of GFP-h, *ermo1-1*, and *ermo2* plants were transformed with each chimeric gene for transient expression of *KAM1ΔC-mRFP*, *Ara6-mRFP*, and *mRFP-PTS1* by particle bombardment, as described previously (Tamura et al., 2007). Cells were inspected with a confocal laser scanning microscope. The plasmid containing *Ara6-mRFP* cDNA was donated by A. Nakano of the University of Tokyo.

Staining with DAPI, Mito-Tracker, and FM4-64

Seven-day-old seedlings were stained with 2.5 μg/mL DAPI (Wako), 50 μM FM4-64 (Invitrogen), or 0.5 μM Mito-Tracker Red CMXRos for 2 h.

Treatment with Lat B, BFA, and CHX

Stock solutions of reagents used were as follows: 5 mM Lat B in DMSO, 10 mg/mL BFA in ethanol, and 50 mM CHX in DMSO. The 7-d-old seedlings were incubated in Murashige and Skoog medium containing each of inhibitors or solvent as a control and vacuumed for 5 min, followed by incubation at normal growth condition for the indicated time.

Confocal Laser Scanning Microscopy

The fluorescent images were obtained with a confocal laser scanning microscope (LSM510 META; Carl Zeiss) using the 488-nm line of a 40-mW Ar/Kr laser for GFP, the 544-nm line of a 1-mW He/Ne laser for RFPs, Mito-Tracker Red CMXRos, and FM4-64, or the 405-nm line of a laser diode 405 for DAPI with either a 100 × 1.45 numerical aperture oil immersion objective or a 40 × 0.95 numerical aperture dry objective. Images were analyzed with LSM image examiner software (Carl Zeiss) and processed with ImageJ (NIH).

Electron Microscopy

Seven-day-old seedlings of GFP-h, *ermo1-1*, and *ermo2* were fixed for 2 h with 4% (w/v) paraformaldehyde and 1% (v/v) glutaraldehyde in 0.05 M cacodylate buffer, pH 7.4. Procedures for electron microscopy were essentially the same as those described previously (Shimada et al., 2003). The ultrathin sections were examined with a transmission electron microscope (model JEM-1011; JEOL) at 100 kV.

Subcellular Fractionation

Three-week-old plants of GFP-h, *ermo1-1*, *ermo2*, and *mag2-1 mal* (0.3 g) were chopped with a razor blade in a Petri dish on ice in 1.0 mL of chopping buffer that contained 50 mM HEPES-NaOH, pH 7.5, 5 mM EDTA, 0.4 M sucrose, and EDTA-free protease inhibitor cocktail (one tablet per 25 mL; Roche Diagnostic). The protein homogenates were subjected to differential centrifugation to obtain a 1000*g* pellet (P1), 8000*g* pellet (P8), 100,000*g* pellet (P100), and a 100,000*g* supernatant (S100) as described previously (Matsushima et al., 2003). Each fraction was

subjected to SDS-PAGE followed by immunoblot analysis with anti-RD21 antibody.

Immunoblot Analysis

Protein extracts from dry seeds (two grains) of the wild type (Col) and GFP-h, *ermo1-1*, *ermo2*, and *mag2-1* mutants were subjected to SDS-PAGE followed by immunoblot analysis. Immunoreactive signals were detected using an ECL detection system (GE Healthcare Bio-Science). Antibodies used were anti-12S globulin α-subunit (diluted 1:10,000) and anti-RD21 (diluted 1:2000) (Hayashi et al., 2001).

Accession Numbers

Sequence data from this article can be found in the Arabidopsis Genome Initiative or GenBank/EMBL databases under the following accession numbers: *GNL1/ERMO1*, At5g39500; At *SEC24a/ERMO2*, At3g07100; At *SEC24b*, At3g44340; At *SEC24c*, At4g32640; At *SEC24d*, At2g27460; *MAG2*, At3g47700; *MAG2-LIKE*, At1g08400; Pp *Sec24A*, XM_001763080; Pp *Sec24B*, XM_001763171; Pp *Sec24C*, XM_001783238; Pp *Sec24D*, XM_001785918; Dm *Sec24*, NM_136687; Hs *Sec24A*, NM_001042734; Hs *Sec24B*, NM_006323; Hs *Sec24C*, NM_004922; Hs *Sec24D*, NM_014822; *Os04g0129500*, NM_001058626; *Os05g0443300*, NM_001062208; *Os12g0430000*, NM_001073209; Sc *Sec24*, NP_012157; Sc *Iss1*, NP_014349; and Sc *Lst1*, NP_011966.

Supplemental Data

The following materials are available in the online version of this article.

Supplemental Figure 1. Distribution of Endoplasmic Reticulum throughout Epidermal Cells of *Arabidopsis* Seedlings.

Supplemental Figure 2. Abnormal Development of Spherical Bodies with ~1-μm Diameters in Various *ermo1* Tissues.

Supplemental Figure 3. Abnormal Formation of an Aggregate Engulfing Many Spherical Bodies with ~1-μm Diameters in Various *ermo2* Cells.

Supplemental Figure 4. Tissue-Specific Phenotypes of *ermo* Mutants.

Supplemental Figure 5. Spherical Bodies of *ermo1-1* or *ermo2* Disappeared in 6-Week-Old Plants.

Supplemental Figure 6. Young Cells of *ermo2* Did Not Develop the Aggregates.

Supplemental Figure 7. Gross Morphological Phenotypes of *ermo1* and *ermo2* Plants.

Supplemental Figure 8. Spherical Bodies of *ermo1-1* and *ermo2* Are Distinct from Known Organelles.

Supplemental Figure 9. A Schematic Model Showing that GNL1/ERMO1 and SEC24a/ERMO2 Are Involved in Formation of COPI Vesicles on the Golgi Membrane and COPII Vesicles on the ER Membrane.

Supplemental Figure 10. BFA Treatment Induced Spherical Structures in Cultured Tobacco BY-2 Cells.

Supplemental Table 1. Primers Used in This Study.

Supplemental Movie 1. The Spherical Bodies in *ermo1* Cells Move along MFs.

Supplemental Movie 2. The Spherical Bodies in *ermo2* Cells Move along MFs.

ACKNOWLEDGMENTS

We thank Tsuyoshi Nakagawa of Shimane University, Seiichiro Hasezawa of the University of Tokyo, Akihiko Nakano of the University of Tokyo, Chris Hawes of Oxford Brookes University, and Roger Y. Tsien of Howard Hughes Medical Institute for their donations of plasmids and Masao Tasaka and Miyo Morita of Nara Institute of Science and Technology for donation of the NARAMAP marker. We also thank the ABRC for providing seeds of *Arabidopsis* T-DNA insertion mutants (SALK_067415, SALK_091078, and SALK_030701) and the Nottingham Arabidopsis Stock Centre for providing a GABI-KAT line (GK-288E12). This work was supported by Grants-in-Aid for Scientific Research (16085203 and 17107002) from the Ministry of Education, Culture, Sports, Science, and Technology (MEXT) of Japan, by the Global Center of Excellence Program "Formation of a Strategic Base for Biodiversity and Evolutionary Research: from Genome to Ecosystem" of MEXT, and by a research fellowship to R.T.N. from the Japan Society for the Promotion of Science (21001585).

Received April 28, 2009; revised October 9, 2009; accepted October 17, 2009; published November 20, 2009.

REFERENCES

Baldwin, T.C., Handford, M.G., Yuseff, M.I., Orellana, A., and Dupree, P. (2001). Identification and characterization of GONST1, a golgi-localized GDP-mannose transporter in *Arabidopsis*. Plant Cell **13:** 2283–2295.

Baumann, O., and Walz, B. (2001). Endoplasmic reticulum of animal cells and its organization into structural and functional domains. Int. Rev. Cytol. **205:** 149–214.

Bell, C.J., and Ecker, J.R. (1994). Assignment of 30 microsatellite loci to the linkage map of Arabidopsis. Genomics **19:** 137–144.

Clough, S.J., and Bent, A.F. (1998). Floral dip: A simplified method for Agrobacterium-mediated transformation of *Arabidopsis thaliana*. Plant J. **16:** 735–743.

Dabora, S.L., and Sheetz, M.P. (1988). The microtubule-dependent formation of a tubulovesicular network with characteristics of the ER from cultured cell extracts. Cell **54:** 27–35.

De Craene, J.O., Coleman, J., Estrada de Martin, P., Pypaert, M., Anderson, S., Yates III, J.R., Ferro-Novick, S., and Novick, P. (2006). Rtn1p is involved in structuring the cortical endoplasmic reticulum. Mol. Biol. Cell **17:** 3009–3020.

Dreier, L., and Rapoport, T.A. (2000). In vitro formation of the endoplasmic reticulum occurs independently of microtubules by a controlled fusion reaction. J. Cell Biol. **148:** 883–898.

Estrada de Martin, P., Du, Y., Novick, P., and Ferro-Novick, S. (2005b). Ice2p is important for the distribution and structure of the cortical ER network in *Saccharomyces cerevisiae*. J. Cell Sci. **118:** 65–77.

Estrada de Martin, P., Novick, P., and Ferro-Novick, S. (2005a). The organization, structure, and inheritance of the ER in higher and lower eukaryotes. Biochem. Cell Biol. **83:** 752–761.

Estrada, P., Kim, J., Coleman, J., Walker, L., Dunn, B., Takizawa, P., Novick, P., and Ferro-Novick, S. (2003). Myo4p and She3p are required for cortical ER inheritance in *Saccharomyces cerevisiae*. J. Cell Biol. **163:** 1255–1266.

Faso, C., Chen, Y.-N., Tamura, K., Held, M., Zemelis, S., Marti, L., Saravanan, R., Hummel, E., Kung, L., Miller, E., Hawes, C., and Brandizzi, F. (2009). A missense mutation in the *Arabidopsis* COPII coat protein Sec24A induces the formation of clusters of the endoplasmic reticulum and Golgi apparatus. Plant Cell **21:** 3655–3671.

Fuji, K., Shimada, T., Takahashi, H., Tamura, K., Koumoto, Y., Utsumi, S., Nishizawa, K., Maruyama, N., and Hara-Nishimura, I. (2007). *Arabidopsis* vacuolar sorting mutants (green fluorescent seed) can be identified efficiently by secretion of vacuole-targeted green fluorescent protein in their seeds. Plant Cell **19:** 597–609.

Hara-Nishimura, I., Matsushima, R., Shimada, T., and Nishimura, M. (2004). Diversity and formation of endoplasmic reticulum-derived compartments in plants. Are these compartments specific to plant cells? Plant Physiol. **136:** 3435–3439.

Hayashi, Y., Yamada, K., Shimada, T., Matsushima, R., Nishizawa, N.K., Nishimura, M., and Hara-Nishimura, I. (2001). A proteinase-storing body that prepares for cell death or stresses in the epidermal cells of Arabidopsis. Plant Cell Physiol. **42:** 894–899.

Hicke, L., Yoshihisa, T., and Schekman, R. (1992). Sec23p and a novel 105-kDa protein function as a multimeric complex to promote vesicle budding and protein transport from the endoplasmic reticulum. Mol. Biol. Cell **3:** 667–676.

Higaki, T., Sano, T., and Hasezawa, S. (2007). Actin microfilament dynamics and actin side-binding proteins in plants. Curr. Opin. Plant Biol. **10:** 549–556.

Hu, J., Shibata, Y., Voss, C., Shemesh, T., Li, Z., Coughlin, M., Kozlov, M.M., Rapoport, T.A., and Prinz, W.A. (2008). Membrane proteins of the endoplasmic reticulum induce high-curvature tubules. Science **319:** 1247–1250.

Kaiser, C.A., and Schekman, R. (1990). Distinct sets of SEC genes govern transport vesicle formation and fusion early in the secretory pathway. Cell **61:** 723–733.

Kano, F., Kondo, H., Yamamoto, A., Tanaka, A.R., Hosokawa, N., Nagata, K., and Murata, M. (2005). The maintenance of the endoplasmic reticulum network is regulated by p47, a cofactor of p97, through phosphorylation by cdc2 kinase. Genes Cells **10:** 333–344.

Klausner, R.D., Donaldson, J.G., and Lippincott-Schwartz, J. (1992). Brefeldin A: Insights into the control of membrane traffic and organelle structure. J. Cell Biol. **116:** 1071–1080.

Konieczny, A., and Ausubel, F.M. (1993). A procedure for mapping Arabidopsis mutations using co-dominant ecotype-specific PCR-based markers. Plant J. **4:** 403–410.

Li, L., Shimada, T., Takahashi, H., Ueda, H., Fukao, Y., Kondo, M., Nishimura, M., and Hara-Nishimura, I. (2006). MAIGO2 is involved in exit of seed storage proteins from the endoplasmic reticulum in *Arabidopsis thaliana*. Plant Cell **18:** 3535–3547.

Matsushima, R., Fukao, Y., Nishimura, M., and Hara-Nishimura, I. (2004). NAI1 gene encodes a basic-helix-loop-helix-type putative transcription factor that regulates the formation of an endoplasmic reticulum-derived structure, the ER body. Plant Cell **16:** 1536–1549.

Matsushima, R., Hayashi, Y., Kondo, M., Shimada, T., Nishimura, M., and Hara-Nishimura, I. (2002). An endoplasmic reticulum-derived structure that is induced under stress conditions in Arabidopsis. Plant Physiol. **130:** 1807–1814.

Matsushima, R., Hayashi, Y., Yamada, K., Shimada, T., Nishimura, M., and Hara-Nishimura, I. (2003). The ER body, a novel endoplasmic reticulum-derived structure in Arabidopsis. Plant Cell Physiol. **44:** 661–666.

Mayer, U., Buttner, G., and Jurgens, G. (1993). Apical-basal pattern formation in the Arabidopsis embryo: Studies on the role of the gnom gene. Development **117:** 149–162.

Mayer, U., Torres Ruiz, R.A., Berleth, T., Misera, S., and Jurgens, G. (1991). Mutations affecting body organization in the Arabidopsis embryo. Nature **353:** 402–407.

Miller, E.A., Beilharz, T.H., Malkus, P.N., Lee, M.C., Hamamoto, S., Orci, L., and Schekman, R. (2003). Multiple cargo binding sites on the COPII subunit Sec24p ensure capture of diverse membrane proteins into transport vesicles. Cell **114:** 497–509.

Mitsuhashi, N., Shimada, T., Mano, S., Nishimura, M., and Hara-Nishimura, I. (2000). Characterization of organelles in the vacuolar-sorting pathway by visualization with GFP in tobacco BY-2 cells. Plant Cell Physiol. **41:** 993–1001.

Nakagawa, T., et al. (2007). Improved Gateway binary vectors: High-performance vectors for creation of fusion constructs in transgenic analysis of plants. Biosci. Biotechnol. Biochem. **71:** 2095–2100.

Nziengui, H., Bouhidel, K., Pillon, D., Der, C., Marty, F., and Schoefs, B. (2007). Reticulon-like proteins in *Arabidopsis thaliana*: Structural organization and ER localization. FEBS Lett. **581:** 3356–3362.

Okita, T.W., and Rogers, J.C. (1996). Compartmentation of proteins in the endomembrane system of plant cells. Annu. Rev. Plant Physiol. Plant Mol. Biol. **47:** 327–350.

Prinz, W.A., Grzyb, L., Veenhuis, M., Kahana, J.A., Silver, P.A., and Rapoport, T.A. (2000). Mutants affecting the structure of the cortical endoplasmic reticulum in *Saccharomyces cerevisiae*. J. Cell Biol. **150:** 461–474.

Renault, L., Guibert, B., and Cherfils, J. (2003). Structural snapshots of the mechanism and inhibition of a guanine nucleotide exchange factor. Nature **426:** 525–530.

Richter, S., Geldner, N., Schrader, J., Wolters, H., Stierhof, Y.D., Rios, G., Koncz, C., Robinson, D.G., and Jurgens, G. (2007). Functional diversification of closely related ARF-GEFs in protein secretion and recycling. Nature **448:** 488–492.

Ritzenthaler, C., Nebenfuhr, A., Movafeghi, A., Stussi-Garaud, C., Behnia, L., Pimpl, P., Staehelin, L.A., and Robinson, D.G. (2002). Reevaluation of the effects of brefeldin A on plant cells using tobacco Bright Yellow 2 cells expressing Golgi-targeted green fluorescent protein and COPI antisera. Plant Cell **14:** 237–261.

Robineau, S., Chabre, M., and Antonny, B. (2000). Binding site of brefeldin A at the interface between the small G protein ADP-ribosylation factor 1 (ARF1) and the nucleotide-exchange factor Sec7 domain. Proc. Natl. Acad. Sci. USA **97:** 9913–9918.

Saint-Jore, C.M., Evins, J., Batoko, H., Brandizzi, F., Moore, I., and Hawes, C. (2002). Redistribution of membrane proteins between the Golgi apparatus and endoplasmic reticulum in plants is reversible and not dependent on cytoskeletal networks. Plant J. **29:** 661–678.

Satiat-Jeunemaitre, B., Cole, L., Bourett, T., Howard, R., and Hawes, C. (1996). Brefeldin A effects in plant and fungal cells: Something new about vesicle trafficking? J. Microsc. **181:** 162–177.

Shibata, Y., Voss, C., Rist, J.M., Hu, J., Rapoport, T.A., Prinz, W.A., and Voeltz, G.K. (2008). The reticulon and DP1/Yop1p proteins form immobile oligomers in the tubular endoplasmic reticulum. J. Biol. Chem. **283:** 18892–18904.

Shimada, T., Fuji, K., Tamura, K., Kondo, M., Nishimura, M., and Hara-Nishimura, I. (2003). Vacuolar sorting receptor for seed storage proteins in *Arabidopsis thaliana*. Proc. Natl. Acad. Sci. USA **100:** 16095–16100.

Shimada, T., Koumoto, Y., Li, L., Yamazaki, M., Kondo, M., Nishimura, M., and Hara-Nishimura, I. (2006). AtVPS29, a putative component of a retromer complex, is required for the efficient sorting of seed storage proteins. Plant Cell Physiol. **47:** 1187–1194.

Staehelin, L.A. (1997). The plant ER: A dynamic organelle composed of a large number of discrete functional domains. Plant J. **11:** 1151–1165.

Tamura, K., Shimada, T., Kondo, M., Nishimura, M., and Hara-Nishimura, I. (2005). KATAMARI1/MURUS3 is a novel Golgi membrane protein that is required for endomembrane organization in Arabidopsis. Plant Cell **17:** 1764–1776.

Tamura, K., Takahashi, H., Kunieda, T., Fuji, K., Shimada, T., and Hara-Nishimura, I. (2007). Arabidopsis KAM2/GRV2 is required for proper endosome formation and functions in vacuolar sorting and determination of the embryo growth axis. Plant Cell **19:** 320–332.

Teh, O.K., and Moore, I. (2007). An ARF-GEF acting at the Golgi and in selective endocytosis in polarized plant cells. Nature **448:** 493–496.

Tolley, N., Sparkes, I.A., Hunter, P.R., Craddock, C.P., Nuttall, J., Roberts, L.M., Hawes, C., Pedrazzini, E., and Frigerio, L. (2008). Overexpression of a plant reticulon remodels the lumen of the cortical endoplasmic reticulum but does not perturb protein transport. Traffic **9:** 94–102.

Tse, Y.C., Mo, B., Hillmer, S., Zhao, M., Lo, S.W., Robinson, D.G., and Jiang, L. (2004). Identification of multivesicular bodies as prevacuolar compartments in *Nicotiana tabacum* BY-2 cells. Plant Cell **16:** 672–693.

Uchiyama, K., Jokitalo, E., Kano, F., Murata, M., Zhang, X., Canas, B., Newman, R., Rabouille, C., Pappin, D., Freemont, P., and Kondo, H. (2002). VCIP135, a novel essential factor for p97/p47-mediated membrane fusion, is required for Golgi and ER assembly in vivo. J. Cell Biol. **159:** 855–866.

Uchiyama, K., Totsukawa, G., Puhka, M., Kaneko, Y., Jokitalo, E., Dreveny, I., Beuron, F., Zhang, X., Freemont, P., and Kondo, H. (2006). p37 is a p97 adaptor required for Golgi and ER biogenesis in interphase and at the end of mitosis. Dev. Cell **11:** 803–816.

Ueda, T., Uemura, T., Sato, M.H., and Nakano, A. (2004). Functional differentiation of endosomes in Arabidopsis cells. Plant J. **40:** 783–789.

Vedrenne, C., and Hauri, H.P. (2006). Morphogenesis of the endoplasmic reticulum: Beyond active membrane expansion. Traffic **7:** 639–646.

Voeltz, G.K., Prinz, W.A., Shibata, Y., Rist, J.M., and Rapoport, T.A. (2006). A class of membrane proteins shaping the tubular endoplasmic reticulum. Cell **124:** 573–586.

Waterman-Storer, C.M., and Salmon, E.D. (1998). Endoplasmic reticulum membrane tubules are distributed by microtubules in living cells using three distinct mechanisms. Curr. Biol. **8:** 798–806.

Wee, E.G., Sherrier, D.J., Prime, T.A., and Dupree, P. (1998). Targeting of active sialyltransferase to the plant Golgi apparatus. Plant Cell **10:** 1759–1768.

Zeghouf, M., Guibert, B., Zeeh, J.C., and Cherfils, J. (2005). Arf, Sec7 and brefeldin A: A model towards the therapeutic inhibition of guanine nucleotide-exchange factors. Biochem. Soc. Trans. **33:** 1265–1268.